Design Consideration for Modeless Integrated Circuit Substrates Using Planar Periodic Patches

Hung-Yu David Yang, *Fellow, IEEE*, Reonghee Kim, *Student Member, IEEE*, and David R. Jackson, *Fellow, IEEE*

***Abstract*—In recent years, there has been significant interest in complete surface-wave elimination (meaning in all possible directions) through the use of periodic elements incorporated into integrated circuit structures. However, to date there is no comprehensive theory for the design of the surface-wave bandgap, and it also appears that leaky modes with complex propagation constants that may exist on the planar periodic structures have not been properly taken into account. As shown here, fast periodic leaky modes may exist within a surface-wave bandgap zone. These leaky modes may result in more energy loss and crosstalk than the surface-wave modes and should be taken into account in circuit design. This paper presents theory and experimental validation for guided surface-wave and leaky modes on a printed circuit structure consisting of planar periodic metal patches over a grounded substrate. The existence of surface-wave bandgaps and leaky modes is attributed to either element resonances or the weakly bounded dielectric slab modes. It is also found that fast periodic leaky modes may exist within a surface-wave bandgap zone. Design procedures for achieving a complete surface-wave bandgap without leaky-modes are outlined and examples are given.**

***Index Terms*—Bandgap, integrated circuit, leaky wave, microstrip, periodic structures, photonic band gap, surface wave.**

I. Introduction

In RECENT years, there has been significant renewed interest in microwave applications of wave bandgap technology [1]–[3], particularly in two- or three-dimensional periodic structures. Printed circuit elements placed on a dielectric or semiconductor substrate are known to generate surface-wave modes (or dielectric-slab modes). There are two major effects of the surface-wave mode generation. First, surface-wave modes propagating laterally are distinct from space waves and are considered losses in integrated circuits. Second, crosstalk between devices printed on the surface of the substrate may be significant due to the surface-wave interaction. It is therefore often desirable to eliminate or minimize the surface-wave effects. A few years ago, the use of artificial periodic materials as the integrated-circuit substrates was proposed in order to eliminate surface-wave modes within a frequency bandgap zone [1]. It was concluded, however, that with common material (dielectric) periodic elements, a complete surface-wave elimination in all directions is not feasible [2], [3]. The main reason is that the surface-wave phase constant variation with respect to the angle of propagation ϕ (measured in the array plane) is not dramatic. As a result, the Bragg diffraction condition cannot be satisfied in all directions (since, for a rectangular lattice, the "effective periodicity" depends significantly on angle). It was found recently that the use of metallic periodic patches and vias could result in a surface-wave bandgap in all directions [4] at low frequencies. However, this bandgap is due to the prevention of the fundamental TM mode propagation largely via the element design rather than Bragg diffraction.

This paper will demonstrate that a complete bandgap is possible for all angles of propagation ϕ when using periodic metallic patch elements. The complete bandgap is due to pronounced element resonances, which in turn result in a large variation of phase constant over a short frequency range. The use of metallic elements allows for the creation of frequency bandgap edges that are relatively insensitive to angle (and hence a surface-wave bandgap can be created for all angles [5]. Once the phase constant of a bound mode (a mode having fields that decay vertically) is close to the Bragg diffraction condition ($\beta a = \pi$, with β the phase constant and a the periodicity), the corresponding mode becomes a bound complex mode that is highly attenuating. The mode is no longer a propagating mode but an evanescent mode that does not carry power. The frequency band within which the mode is complex is a surface-wave bandgap. However, as shown here, leaky modes that are fast waves (with respect to free space) with a small attenuation constant may also exist inside the bandgap region. In contrast to a complex evanescent mode, a leaky mode will leak power into space, resulting in significant power loss for the circuits. A leaky mode may also cause interference with other circuits or devices placed above the integrated circuit. In order to have a complete understanding of mode propagation on artificial periodic substrates, the leaky modes should be taken into account properly.

In experimental verification of bandgaps, a transmitter and receiver are often placed at opposite sides of the planar structure. A low signal reception is assumed to indicate the existence of a surface-wave bandgap. However, it is shown here that there may exist leaky-mode excitation at frequencies inside the surface-wave bandgap. In this case, the signal reception may still be low, but power loss from the circuit is not avoided; rather, it is redirected into space. Furthermore, the leaky mode may have a small attenuation constant and hence propagate to a significant distance at certain frequencies, resulting in crosstalk that

Manuscript received February 20, 2000; revised August 21, 2000. This work was supported in part by the National Science Foundation under Grant NSF ECE 96-14469.

H.-Y. D. Yang and R. Kim are with the Department of Electrical Engineering and Computer Science, University of Illinois at Chicago, Chicago, IL 60637 USA.

D. R. Jackson is with the Department of Electrical and Computer Engineering, University of Houston, Houston, TX 77004 USA.

Publisher Item Identifier S 0018-9480(00)10710-0.

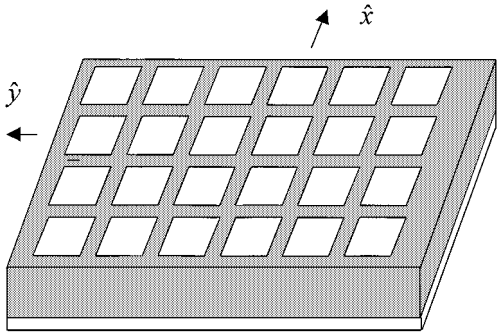

Fig. 1. Planar periodic square patch array on a grounded dielectric substrate. Array period is $a \times a$. Patch length (width) is L.

could potentially be as serious as that from the surface-wave modes. In this paper, we clarify the fact that leaky modes may exist within the surface-wave bandgap. In order to utilize the surface-wave bandgap for loss reduction, it is necessary to also eliminate the leaky modes within the bandgap, creating a complete mode bandgap.

A full-wave integral equation moment-method technique applicable to the analysis of infinite arrays of microstrip element [6], [7] is applied here to find the surface-wave mode and leaky-mode (complex) wavenumbers. The mode diagrams (wavenumber versus frequency) for the periodic metal patch structures are investigated. The surface-wave bandgaps and leaky modes are explained based on element resonances and perturbations of the slab mode of the structure. Measurements of wave transmission through the artificial substrate are performed in order to validate the predicted surface-wave stopband and leaky-mode effects. The guidelines for designing a complete bandgap without surface-wave modes or leaky modes are described, and design examples are given.

II. Analytic and Numerical Methods

The analysis outlined here pertains to wave propagation along a single grounded dielectric slab that has planar periodic metallic elements printed on the interface. An extension to multilayer structures is straightforward. A patch array on a grounded slab structure is shown in Fig. 1. The geometry is assumed planar and infinite. The pertinent problem is analyzed through the use of an electric-field integral-equation formulation in conjunction with the method of moments [6], [7].

Assuming that the metallic elements are thin, the electric-field integral equation for the pertinent problem is

$$\underline{E}(\underline{r}) = \iint_s [G(\underline{r}, \underline{r}')] \cdot \underline{J}(\underline{r}')d \tag{1}$$

where the surface integral is over only one of the periodic elements in a unit cell, having current density $\underline{J}(r')$. The dyadic Green's function, giving the transverse field components for a layered media, is expressed as

$$[G(\underline{r}, \underline{r}'] = \begin{bmatrix} G_{xx}(\underline{r}, \underline{r}') & G_{xy}(\underline{r}, \underline{r}') \\ G_{yx}(\underline{r}, \underline{r}') & G_{yy}(\underline{r}, \underline{r}') \end{bmatrix}. \tag{2}$$

Since the structure is periodic, Floquet's theorem is applied to simplify the problem to the fields within a unit cell. The cross section of the rectangular unit cell includes the region $-a/2 \le x \le a/2$ and $-b/2 \le y \le b/2$, where a and b are the periodicities along the x and y directions, respectively. For the metallic patch structure in Fig. 1, a rectangular microstrip patch having length L along the x axis and width W along the y axis is at the center of the unit cell. (For the results presented later, a square lattice and patch are assumed, so that $a = b$ and $W = L$.) For planar periodic structures, the components of the dyadic Green's function may be expressed in terms of Floquet space harmonics modes (a plane-wave expansion) [6] as

$$G_{ij}(\underline{r}, \underline{r}') = \frac{1}{ab} \sum_{m=-\infty}^{\infty} \sum_{n=-\infty}^{\infty} \tilde{G}_{ij} \cdot (k_x, k_y, z, z') e^{-jk_x(x-x')-jk_y(y-y')}. \tag{3}$$

In this equation, i and j are either x or y, and the wavenumbers are defined as $k_{xm} = k_{x0} + (2\pi m/a)$, $k_{yn} = k_{y0} + (2\pi n/a)$, where k_{x0} and k_{y0} are the fundamental propagation wavenumbers (wavenumbers of the fundamental (zero-order) Floquet harmonics) in the x and y directions, respectively. $\tilde{G}_{ij}$ is the spectral Green's function component and is a function of the spectral variables k_x and k_y, z and z', and the material parameters. This spectral Green's function term for a multilayer periodic structure is the same as that for a single (nonperiodic) element and was derived with a spectral matrix method [1].

A Galerkin moment-method procedure is applied numerically to determine the current distribution on the patch element in the unit cell. Entire-domain basis functions based on patch cavity modes [6] are used to represent the current density in (1), and the inner products of the resulting electric fields with a set of testing functions (the same entire-domain basis functions) are then set to zero in order to convert the electric field integral equation into the matrix equation $[Z][I] = [\ ]$. The matrix elements are in terms of a double infinite series in a similar form as that in (3) and are evaluated numerically. A nontrivial solution for the current requires the matrix determinant to be zero, which results in a characteristic equation. The eigenvalues (propagation wavenumbers) $k_\rho = \beta - j\alpha$ are obtained from the roots of this equation for a given direction in the phase plane (i.e., for a given ratio of k_{y0}/k_{x0} or, equivalently, a given angle ϕ, where $k_{x0} = k_\rho \cos\phi$ and $k_{y0} = k_\rho \sin\phi$). When the propagation wavenumber is purely real (for a lossless structure), the corresponding mode is a bound mode. When the wavenumber is a complex value, the mode may be either an attenuating slow wave (an evanescent surface-wave mode in the bandgap) or a radiating leaky mode [8].

Numerical results for the metallic patch structure are based on nine entire-domain basis functions for each current component. In order to provide code validation, results were also obtained by using subdomain basis functions (rooftop functions), and a very good agreement was found.

III. Results and Discusssion

A. Modal Analysis for Periodic Square Patches

An example of the $\beta - f$ diagram for the planar patch array in Fig. 1 is shown in Fig. 2. The substrate is 1.27 mm thick with dielectric constant 10.2. The square patches are 6 mm long, and

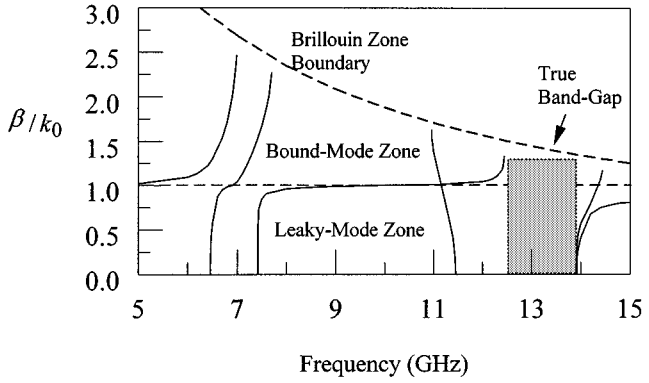

Fig. 2. Normalized phase constant β/k_0 versus frequency for waves on the planar periodic patch array of Fig. 1. Propagation is in the $\chi(\phi = 0)$ direction.

the array spacing (period) is 8 mm in both principal directions. The propagation is in the x direction for the results in Fig. 2. The propagation wavenumbers shown in the plot are for the fundamental Floquet wavenumber k_{x0} unless otherwise noted.

Only physical modal solutions are shown in this plot. A physical modal solution is one for which the Floquet space harmonics are bound (decaying vertically) if the Floquet wavenumbers are in the slow-wave region ($|\beta| > k_0$) or if they are in the fast-wave region ($|\beta| < k_0$) but correspond to backward waves (the power flow or group velocity of the Floquet mode is in the opposite direction to the phase velocity). On the other hand, a physical modal solution will have improper Floquet space harmonics (with fields that grow vertically) if those Floquet harmonics correspond to forward waves in the fast-wave region.

Both the patch size and the array period determine the bandgap locations. It is seen that at low frequencies, where the patch electrical length is much less than a wavelength, the guided wave is similar to that for an unloaded dielectric substrate (β/k_0 is close to, but greater than, 1). When the frequency increases and approaches the first patch resonance frequency, the phase constant increases dramatically toward the edge of the Brillouin zone boundary, which corresponds to $\beta a = \pi$. Near the resonance, the patch array elements tend to electrically interconnect, as observed in the stopband of a frequency-selective surface [9], [10].

When the phase constant is close to the Bragg condition ($\beta a \approx \pi$), at the edge of the Brillouin zone, the bound mode turns into a highly attenuating wave with a complex wavenumber and the mode is said to be in the bandgap zone. Note that due to the patch resonance, the bandgap starts at a frequency much smaller than for the case of periodic material elements (almost half the frequency for the same period a). The first two modal solutions are associated with the first two patch resonances, the (1,0) and (0,1) patch modes (which have the same resonance frequencies for the case of square patches). It is interesting to observe that in contrast to the first bound mode that has no cutoff, the second bound mode becomes a physical but improper leaky mode ($\beta < k_o$) below its cutoff. This phenomenon can be explained by consideration of the patch currents. For wave propagation in the x direction, the first mode is associated with the patch (1,0) mode (with a large current in the x direction). This (1,0) patch mode results in a TM-like mode (H-field perpendicular to the direction of propagation), similar to the TM mode of a grounded slab at low frequencies, and therefore without a cutoff frequency. The second mode is associated with the patch (0,1) mode (with a large current in the y direction). This (0,1) patch mode results in a TE-like mode. For a grounded slab without a periodic loading, the lowest TE mode (the TE_1 mode) has a nonzero cutoff frequency, and TE_1 mode below cutoff becomes a nonphysical improper real solution (an improper solution with a real-valued propagation wavenumber). However, the periodic loading turns the improper real mode into a physical fast leaky mode [11].

The next modal bandgap edge occurs at about 11 GHz, which is due to the patch (1,1) mode resonance. The Floquet harmonic of the (1,1) mode shown in the plot is a backward wave, since the power flow is in the negative x direction for this mode.

It is seen from Fig. 2 that there also exists a large frequency band (8–11 GHz) where there exists either a fast leaky mode or a weakly bound surface-wave type of mode with ($\beta \approx k_0$. The leaky mode gradually turns into the bound mode as the frequency increases in this band. Because the phase constant of this mode is close to k_0 over most of the frequency range, this mode is referred to as a "TEM-like" mode. Practically, in the leaky-mode region, this mode has the potential to cause significant radiation and power loss in integrated circuits. The existence of a surface-wave bandgap does not by itself, therefore, necessarily imply reduced circuit losses.

As the frequency increases beyond the (1,1)-patch mode resonance, the TEM-like mode turns into a nonpropagating evanescent mode (the fourth bandgap edge) at about 12.45 GHz. This bandgap edge, unlike the others, is not due to patch resonances and is similar to the bandgap edges for a periodic structure loaded with material blocks [1].

Note that for the example given, the first TE mode of the slab without periodic loading (the TE1 mode) has a cutoff at about 19.47 GHz, and that all the modes become leaky (since $a \geq \lambda_0/2$) for $f \geq 18.75$ GHz. Practically, the operating frequency should be below both of these two frequencies. It is seen that there is a frequency band (from 12.45 to 13.9 GHz) where there is no bound or leaky mode. This frequency region is a true bandgap. The next two modes after this bandgap are related to the patch (2,0) and (0,2) modes, respectively. It is concluded from Fig. 2 that for this geometry, the bandgap edges are explainable from the existence of either patch resonant modes or the TEM-like mode.

Experimental results for the case given in Fig. 2 are shown in Fig. 3. A patch array having the structure shown in Fig. 1 is fabricated with a standard photolithography technique, and two probes are soldered at the opposite substrate edges. The transmission across the substrate is measured by an HP-8510C to determine the transmission properties. It is interesting to observe that at around 7 GHz, there is a sudden drop in transmission, a result of the first bandgap predicted in Fig. 2. When the second bound mode starts to propagate immediately after 7 GHz, there is a slight increase in transmission, which agrees with the theoretical results in Fig. 2. It is also interesting to observe that transmission starts to increase beyond 8 GHz. As predicted in Fig. 2, this is due to the leaky mode attenuation constant's decreasing

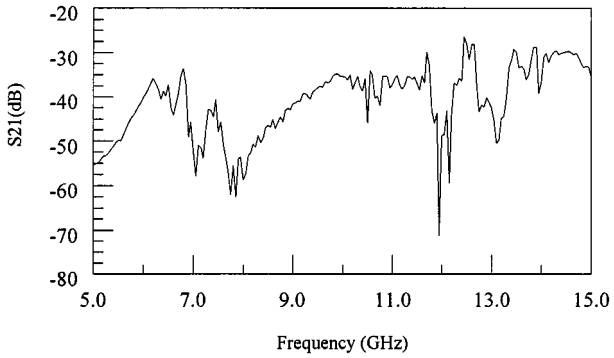

Fig. 3. Measured power reception across the dielectric slab for the case in Fig. 2.

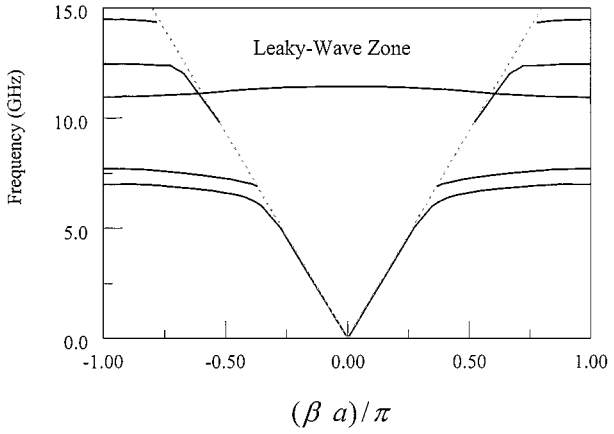

Fig. 4. The $f - \beta$ diagram for the example in Fig. 2.

as the mode evolves into a bound mode. The measured results show that there is a low-reception zone around 8 GHz. The theoretical results in Fig. 2 suggest that this may be due to the fact that the frequency is within the surface-wave bandgap region, while also in a region where the leaky mode is attenuating fairly rapidly (corresponding to radiation into space). It is seen from the measured data that there is also a low-reception zone around 13 GHz. This frequency band, according to the theoretical prediction (in Fig. 2), is in the true bandgap zone (region of modeless propagation without surface-wave or leaky-wave modes). We may define this frequency band as a useful bandgap for integrated circuits.

The mode diagram in Fig. 2 is for positive phase constants within the first Brillouin zone. A more conventional plot of the mode diagram for a periodic structure is shown in Fig. 4. Note that β is periodic with a period $2\pi/a$, and frequency is an even function of β in this plot. The Brillouin-zone boundary in Fig. 2 corresponds to the right edge of the plot in Fig. 4, at $\beta a = \pi$. The leaky-wave boundary in Fig. 4 corresponds to the region below the $\beta = k_0$ line in Fig. 2. It is seen that for frequency less than 15 GHz, there are four improper but physical leaky modes and one proper physical leaky mode [the (1,1) mode with backward propagation]. The results given in Figs. 2 and 3 are for propagation in the x $(\phi = 0)$ direction only. A bandgap that exists in one direction may not be present for other directions. For planar structures, one is interested in wave propagation in all possible

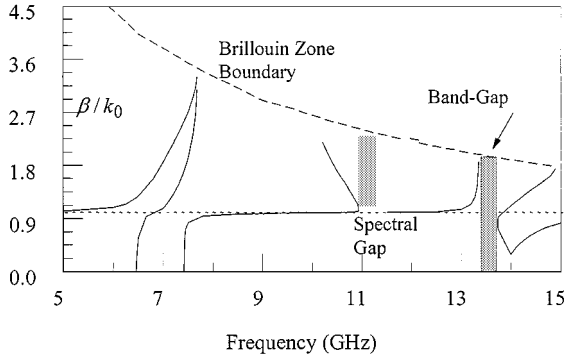

Fig. 5. Normalized phase constant (β/k_0) versus frequency for waves on the planar periodic patch array of Fig. 1. Propagation is in the diagonal $(\phi = 45°)$ direction.

planar directions (ϕ from 0 to 360°). For square patches and lattice, due to symmetry, the propagation information for ϕ from 0 to 45° is sufficient. For a square lattice, the propagation characteristics in the $\phi = 0$ and $\phi = 45°$ directions are the most distinct. A comparison of the mode diagrams for these two directions provides general information about the mode characteristics in all possible directions.

Fig. 5 shows the $\beta - f$ diagram for the same case in Fig. 2, except that $\phi = 45°$. Comparing Figs. 2 and 5, we can see that the general propagation characteristics are similar in the two different directions. The first three modes relate to the patch (1,0), (0,1), and (1,1) modes. The next three modes relate to the TEM-like mode and the patch (2,0) and (0,2) modes, respectively.

There are three main differences for the modes propagating in the two different directions. First, for propagation in the $\phi = 45°$ direction, the first two (patch) modes merge together at the frequency where they turn into complex evanescent modes (at the Brillouin boundary). Second, as shown in Fig. 5, there is "spectral gap" (not a Bragg diffraction bandgap) for the TEM-like mode after about 11 GHz where this mode intersects the patch (1,1) mode. In this gap region, the TEM-like solution is not found. Third, there is a true bandgap around 13.5 GHz within which there are no bound or leaky modes. This bandgap overlaps with that in the $\phi = 0$ direction (Fig. 2), suggesting that there exists a true bandgap in all directions, within which there are no bound or leaky modes that can propagate in any direction.

Experimental results for the case given in Fig. 5 are shown in Fig. 6. The structure is the same as that in Fig. 2 except that here the two probes are aligned along the diagonal, at 45° to the x axis. The first measured low-reception zone (from about 7 to 8 GHz) corresponds to the lower region of the surface-wave bandgap (where a leaky mode exists) in Fig. 5. The second low-reception zone at about 11 GHz corresponds to the "spectral gap" predicted in Fig. 5. The third observed low-reception zone corresponds to the true wave bandgap (modeless region) in Fig. 5.

The existence of a complete (meaning omnidirectional) wave bandgap for the patch array structure in Fig. 1 is demonstrated through the electromagnetic band diagram (frequency versus

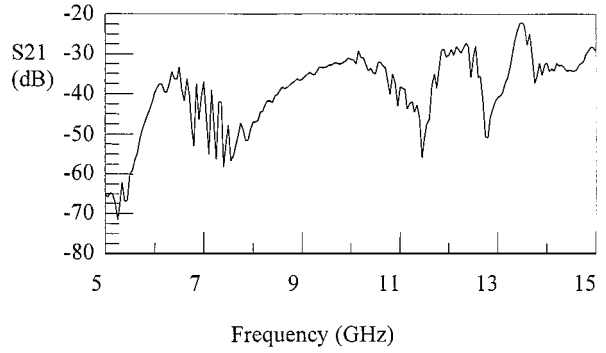

Fig. 6. Measured power reception across the dielectric slab for the case in Fig. 5 (at $\phi = 45°$).

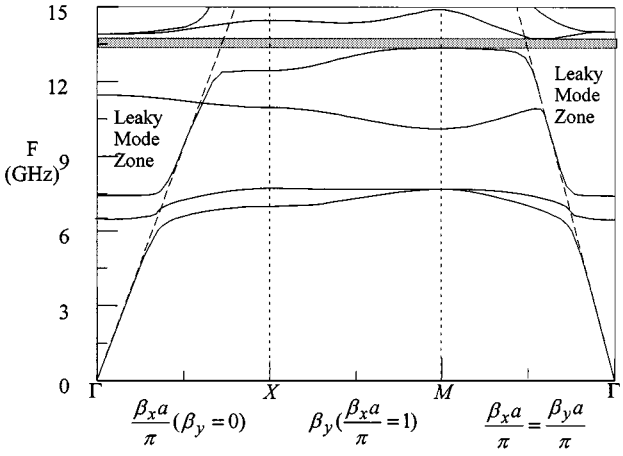

Fig. 7. Two-dimensional guided-wave mode band diagram for periodic square patches on a grounded dielectric substrate. The horizontal axis corresponds to the normalized wavenumber for propagation in different directions. Γ, X, M are symmetric points in the Brillouin zone of the unit cell.

the boundary of the irreducible reciprocal lattice, or the Brillouin-zone spatial boundary) given in Fig. 7. The notations of Γ, X, and M points follow the terminology for the reciprocal lattice of a natural crystal. The first sector of the plot (from Γ to X), plotting frequency versus $\beta_x a/\pi$ from zero to unity, is basically the same as the plot in Fig. 2 except for an axis rotation and different normalization factors. The third (last) sector of the plot (from M to Γ) corresponds to the plot in Fig. 4, plotting frequency versus $\beta_x a/\pi = \beta_y a/\pi$ from unity to zero. The region from X to M plots frequency versus $\beta_y a/\pi$, keeping $\beta_x a/\pi = 1$, and is basically a sampling of the modes in various directions from $\phi = 0$ to $\phi = 45°$. It is seen from Fig. 6 that indeed there is a complete bandgap dictated by the bandgap in the $\phi = 45°$ direction. An important and practical question is whether it is possible in general to design a modeless band (omnidirectional surface-wave bandgap region without any leaky mode) by choosing the parameters of the patch array properly. Some design principles are discussed next.

B. Design Principles for a Complete (Omnidirectional) Wave Bandgap

The previous case shows that for planar metallic patch loading, it is possible to have a large variation of phase constant within a short frequency range due to large electric-field strength and element resonances. Therefore, it is possible that the Bragg condition can be approximately satisfied in all directions at a given frequency. However, the problem with utilizing the patch resonances to obtain a surface-wave bandgap is that there are usually weakly bound modes or leaky modes that exist within the bandgap, as was seen in Figs. 2 and 5. Therefore, such a bandgap is only for the surface-wave modes and may not be useful practically. A complete bandgap, within which all modes are eliminated, including leaky modes, is much more useful. The two modes that determine the edges of a complete bandgap are usually either a weakly bound mode and a patch resonant mode (as for the case in Figs. 2–7) or two patch resonant modes. The latter seems more desirable practically, due to the fact that the element resonances are more controllable by selection of the patch size.

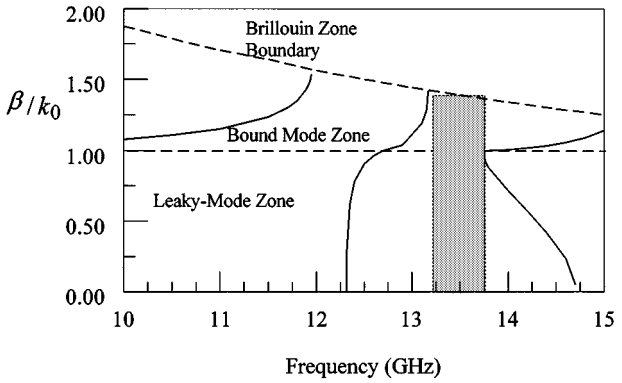

Fig. 8. Normalized phase constant (β/k_0) versus frequency for the first design example of periodic patch array. Propagation is in the $\chi(\phi = 0)$ direction.

The key to the design of a complete wave bandgap (no surface-wave modes and no leaky modes) in all directions is to control the $\beta - f$ curves for the TEM-like mode and patch resonance modes separately. It is seen from Figs. 2 and 5 that there is a large surface-wave bandgap between 8–11 GHz due to the resonance of the (0,1) and (1,1) patch modes, respectively, but within this bandgap there also exists a TEM-like mode that may take the form of either a leaky mode or a weakly bound surface-wave mode. If we can choose the substrate thickness, frequency, or array spacing so that these modes are mostly or completely out of the range of the bandgap edges due to the patch (0,1) and (1,1) modes, a wideband modeless integrated circuit substrate can be obtained.

C. Two Design Examples for a Modeless Substrate

The first design example is for a Duroid substrate 1.27 mm thick with dielectric constant of 10.2 (the same as the previous case). The square patches are 3 mm long (6 mm long for the previous case in Figs. 2–7), and the array spacing (period) is 8 mm in both principal directions (the same as the previous case). Since the patch length is half of that in the previous case, the bandgap edges due to element resonances will scale up (though not exactly in the same proportion as the patch length). However, the TEM-like mode will not change nearly as much. The mode diagram for this case at $\phi = 0°$ is shown in Fig. 8. It is seen that a sizable modeless bandgap exists, where the lower and upper band edges are determined by the resonances of the

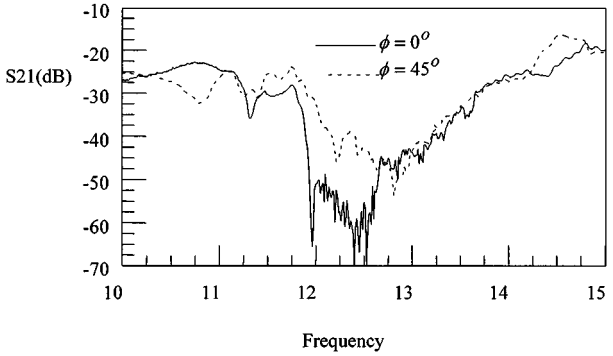

Fig. 9. Measured power reception across the dielectric slab for the first design example. The mode diagram is shown in Fig. 8.

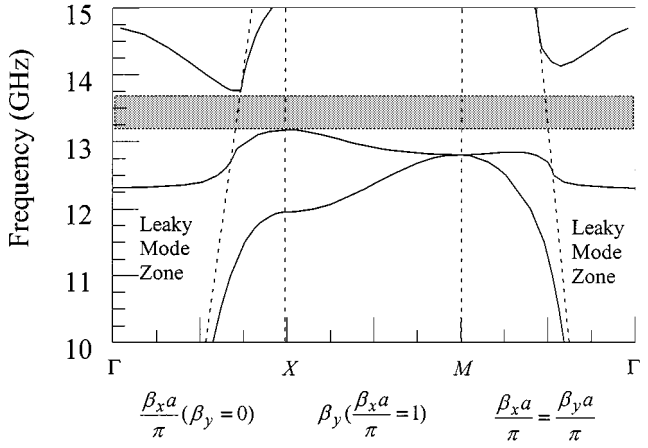

Fig. 10. Mode band diagram for the first design example of the periodic patch array. Note the complete (omnidirectional) bandgap in the shaded strip region.

(0,1) and (1,1) modes (although a TEM-like mode is just beginning to propagate at the upper edge of the bandgap). Hence, this bandgap should be fairly insensitive to direction.

Experiments are carried out to further validate the existence of a complete bandgap for this first design example. The measured results are shown in Fig. 9. They show that there is a low-reception frequency zone from about 12–14 GHz for both the $\phi = 0$ and $\phi = 45°$ cases, confirming the existence of a complete bandgap. The measured results also confirm that at $\phi = 0$, the bound mode corresponding to the patch (0,1) mode is not very significant between 12 and 13 GHz. The measured results show the lowest reception between 12 and 13 GHz, while the modeless bandgap, according to the calculations, extends from about 13.2 to 13.6 GHz. The low reception measured near 12 GHz could be attributed to the fact that the leaky mode in this region is rapidly attenuating. Although this would explain the low reception measured across the circuit board, the radiation into space from such a leaky mode would be undesirable. The corresponding mode band diagram shown in Fig. 10 shows that the bandgap is indeed omnidirectional.

A second design example shows that it is possible to eliminate the TEM-like mode completely within the bandgap by adjusting the substrate thickness. The example is for the same patch length, substrate dielectric constant, and array spacing as for the case in Figs. 2–6, but the substrate thickness is changed to 2.54 mm from 1.27 mm. The mode diagram for this case at

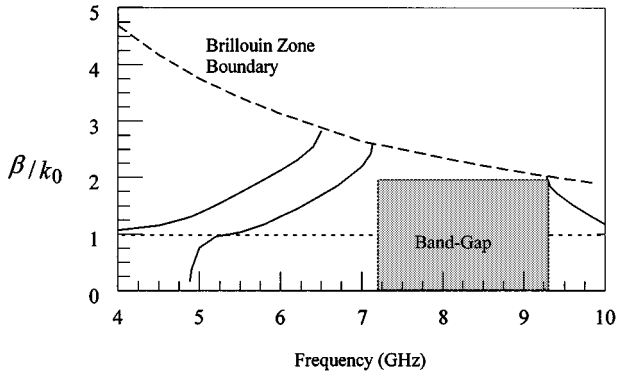

Fig. 11. Normalized phase constant (β/k_0) versus frequency for the second design example of the periodic patch array. Propagation is in the $\chi(\phi = 0)$ direction.

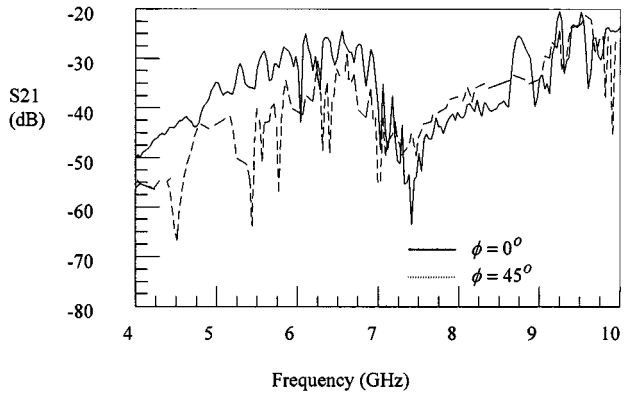

Fig. 12. Measured power reception across the dielectric slab for the second design example. The mode dispersion plot is shown in Fig. 11.

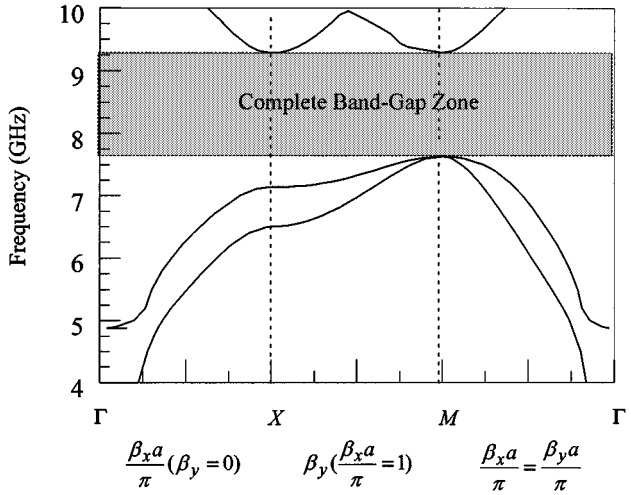

Fig. 13. Mode band diagram for the second design example of the periodic patch array. Note the complete (omnidirectional) bandgap in the shaded strip region.

$\phi = 0$ is shown in Fig. 11. Comparing Figs. 2 and 11, it is seen that the use of a thicker substrate does not change dramatically the bandgap edges due to the patch resonances (i.e., the patch resonance frequencies), but it does eliminate (or push away) the bound slab mode. Consequently, the use of the thicker substrate results in a large modeless bandgap in all directions, at relatively low frequencies. Experiments were carried out to verify

this property for the second design example. A 10×10 patch array with patch size of 6 by 6 mm^2 was printed on the surface of a 100-mil Duroid substrate ($\varepsilon_r = 10.2$). The measured results for power transmission through the substrate are shown in Fig. 12. The results show clearly that there is a low-reception frequency zone from about 7 to 9 GHz for both the $\phi = 0$ and $\phi = 45°$ cases, supporting the theoretical prediction of an omnidirectional modeless bandgap. The corresponding calculated mode band diagram shown in Fig. 13 demonstrates the existence of a complete modeless bandgap within a wide frequency range (about 2 GHz). The large bandgap remains omnidirectional because the bandgap edges in Fig. 11 correspond to the patch resonances of the (0,1) and (1,1) modes and therefore remain widely separated regardless of propagation angle.

IV. Conclusions

This paper addressed the issue of using periodic metallic patches on an integrated-circuit substrate to eliminate surface-wave propagation. It was shown that it is fairly easy to eliminate surface-wave modes completely in a bandgap frequency region by using periodic metallic patch elements, but without careful design, there is usually a leaky mode that limits the extent of a true bandgap. Therefore, from a practical point of view, such a synthesized substrate may not be useful even if surface-wave modes are completely eliminated.

A truly useful integrated-circuit substrate is one where both leaky modes and surface-wave modes are eliminated in all directions, over a moderate range of frequencies. We described design principles to obtain such a modeless substrate where surface-wave modes and leaky-wave modes are eliminated, using metallic patches. A key to the successful design of a large omnidirectional bandgap is to choose the patch dimensions and substrate thickness so that both of the bandgap edges are determined by a Bragg condition arising from patch resonances. The Bragg condition frequencies that determine the bandgap edges then remain widely spaced, for all propagation directions, so that a large omnidirectional bandgap is obtained. Completely modeless artificial substrates were demonstrated with two practical examples. Both theory and experiment confirm the finding. The results in this paper have applications in microwave integrated circuits, where the excitation of substrate modes becomes an important issue.

References

[1] H. Y. D. Yang, "Characteristics of guided and leaky waves on a thin-film structure with planar material gratings," *IEEE Trans. Microwave Theory Tech.*, vol. 45, pp. 428–435, Mar. 1997.

[2] ——, "Surface-wave elimination in integrated circuits with periodic substrates," in *IEEE Int. Microwave Symp. Dig.*, Baltimore, MD, June 1998, pp. 1807–1810.

[3] ——, "Surface-wave elimination in integrated circuits with periodic substrates," *Electromagnetics*, vol. 20, no. 2, pp. 188–193, Mar./Apr. 2000.

[4] D. Sievenpiper, L. Zhang, R. F. Broas, N. G. Alexopoulos, and E. Yablonovitch, "High-impedance electromagnetic surfaces with a forbidden frequency band," *IEEE Trans. Microwave Theory Tech.*, vol. 47, pp. 2059–2074, Nov. 1999.

[5] H. Y. D. Yang, R. Kim, and D. R. Jackson, "Surface-wave band-gap and leaky-waves in integrated circuit structures with planar periodic metallic elements," in *IEEE Int. Microwave Symp. Dig.*, Boston, MA, June 2000, pp. 1521–1524.

[6] D. M. Pozar and D. H. Schaubert, "Analysis of infinite array of rectangular microstrip patches with idealized probe feeds," *IEEE Trans. Antennas Propagat.*, vol. AP-32, pp. 1101–1107, Oct. 1984.

[7] H. Y. Yang and J. A. Castaneda, "Infinite phased arrays of microstrip antennas on generalized anisotropic substrates," *Electromagnetics*, vol. 11, no. 1, pp. 107–124, 1991.

[8] R. E. Collin and F. Z. Zucker, *Antenna Theory Part II*. New York: McGraw-Hill, 1969, ch. 19, pp. 151–258.

[9] R. H. Ott, R. G. Kouyoumjian, and L. Peters, Jr., "Scattering by a two-dimensional periodic arrays of narrow plates," *Radio Sci.*, vol. 2, no. 11, pp. 1327–1359, Nov. 1967.

[10] C. C. Chen, "Scattering by a two-dimensional periodic array of conducting plates," *IEEE Trans. Antennas Propagat.*, vol. AP-18, pp. 660–665, Sept. 1970.

[11] H. Ostner, J. Detlefsen, and D. R. Jackson, "Radiation from one-dimensional dielectric leaky-wave antennas," *IEEE Trans. Antennas Propagat.*, vol. 43, pp. 331–339, Apr. 1995.

Hung-Yu David Yang (S'87–M'88–SM'93–F'00) received the B.S. degree in electrical engineering from National Taiwan University, Taipei, Taiwan, R.O.C., and the M.S. and Ph.D. degrees in electrical engineering from the University of California at Los Angeles in 1982, 1985, and 1988, respectively.

He has been with the Electrical Engineering and Computer Science Department, University of Illinois at Chicago, since 1992 and is currently an Associate Professor. He has published more than 80 technical journal and conference papers. His research interests include computational methods for radiation and scattering from aperiodic structures; microwave, and applications of two- and three-dimensional periodic structures, millimeter-wave, and quasi-optical applications of photonic bandgap materials; passive components in microwave integrated circuits; wave interaction with complex media, and printed circuits and antennas on gyrotropic media. He has been Editor-in-Chief of *Electromagnetics* since 1997.

Prof. Yang is a member of URSI commission B and Sigma Xi. He has been a Technical Program Committee member of the IEEE International Microwave Symposium since 1994. He was an Associate Editor of IEEE Transactions on Antennas and Propagation from 1995–1998.

Reonghee Kim (S'91) received the B.S. degree in science of physics from Kyungpook National University, Korea, in 1991 and the M.S. degree in electro-optics from the University of Dayton, Dayton, OH, in 1996. She is currently pursuing the doctoral degree at the Electrical Engineering and Computer Science Department, University of Illinois at Chicago.

Her research interests include antenna design, microwave circuit, optics, wave interaction with complex media, and applications of photonic bandgap materials.

David R. Jackson (S'83–M'84–SM'95–F'99) was born in St. Louis, MO, on March 28, 1957. He received the B.S.E.E. and M.S.E.E. degrees from the University of Missouri, Columbia, in 1979 and 1981, respectively, and the Ph.D. degree in electrical engineering from the University of California, Los Angeles, in 1985.

From 1985 to 1991, he was an Assistant Profesor in the Department of Electrical and Computer Engineering, University of Houston, TX. From 1991 to 1998, he was an Associate Professor in the same department and, since 1998, he has been a Professor there. He is presently an Associate Editor for the *International Journal of RF and Microwave Computer-Aided Engineering*. He is a past Associate Editor of the *Journal of Radio Science*. His research interests currently include computer-aided design of microstrip antennas and circuits, microstrip antenna analysis and design, periodic structures, and (cover) effects on primed circuit antennas. He is Chair of the Technical Activities Committee for URSI U.S. Commission B.

Dr. Jackson is a past Associate Editor for the IEEE Transactions on Antennas and Propagation. He is a Distinguished Lecturer and Chapter Activities Coordinator for the IEEE AP-S Society.